ACS OMEGA

Article

Cite This: ACS Omega 2018, 3, 14634−14640

http://pubs.acs.org/journal/acsodf

Amperometric Glucose Sensing at Nanomolar Level Using MOF-Encapsulated TiO_2 Platform

Anirban Paul[†,‡] and Divesh N. Srivastava*[,†,‡]

[†]Analytical and Environmental Division and Centralized Instrument Facility and [‡]Academy of Scientific and Innovative Research (AcSIR), CSIR-Central Salt and Marine Chemicals Research Institute, Gijubhai Badheka Marg, Bhavnagar 364002, Gujarat, India

Supporting Information

ABSTRACT: A new synthetic approach is established where both TiO_2 nanoparticles and glucose oxidase (GO_x) are together encapsulated into the cavity of ZIF-8 metal−organic framework (MOF) to fabricate a mediator-free glucose sensor in aqueous media. ZIF-8 possesses high stability both physically and chemically. Moreover, its large surface area and tunable cavity size are supportive to encapsulate both nanoparticles (TiO_2) and enzymes (GO_x). The as-synthesized nanocomposite is methodically characterized by various advanced analytical techniques, which suggests that TiO_2 is uniformly distributed within the cavity of ZIF-8 MOF. High surface area and double-layer capacitance of nanostructured TiO_2 jointly enhance the catalytic biosensor activity. The as-synthesized nanocomposite exhibits commendable stability and is able to detect low-level concentration (80 nM) of glucose in aqueous media by utilizing very low concentration of GO_x (62 μg in 1 mL).

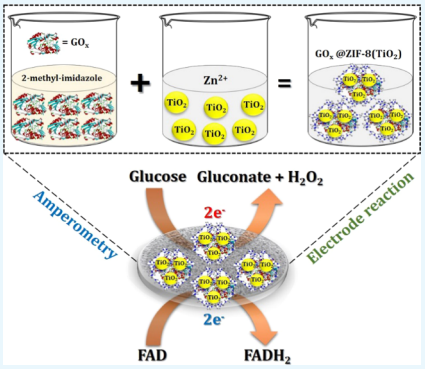

1. INTRODUCTION

Nowadays, diabetes mellitus is known to be the most prevalent chronic disease when compared to other harmful diseases that affect human body. There are few reasons given by the World Diabetes Foundation: the disease occurs mainly due to obesity and lack of physical activity. Moreover, it is occurring frequently due to rapid urbanization and modern lifestyle acquired by people. The disease has a direct effect as it destabilizes the level of blood glucose in our body, which ultimately causes grave health problems including cardiac arrest, kidney function failure, and even deterioration of neurons.[1] Generally, doctors recommend patients suffering from this disease to check their level of blood glucose periodically and to take invasive shots of insulin sporadically to manage the level of blood glucose for a long time.[2] Because the available routine methods are associated with invasive methods such as injection, which is painful, glucose monitoring in a noninvasive way is highly necessary.[3−5] It is been a long time since the first proposal from Clark and Lyon in 1962 regarding the concept of glucose sensing, and still new approaches are being invited by the scientific fraternity. In earlier versions, atmospheric oxygen is used as mediator for glucose sensor response. As technology evolves, new-generation glucose sensor had been introduced according to the demand. As per the current requirement, sophisticated techniques are in high demand, requiring less amount of enzyme and operating noninvasively. Saliva/sweat can be taken as an excellent medium of choice for noninvasive point-of-care glucose monitoring. The state of the art in this area is reviewed by various authors.[6−8] One of the major challenges to date to fabricate sophisticated glucose sensor of such type is the long-term stability of the enzyme. Generally, enzymes, including also glucose oxidase (GOD), are very much sensitive toward pH and temperature. New concepts were introduced to freeze the activity of GO_x by encapsulating into some rigid cavity. Mediator-free direct electron transfer between the electrode and the active center of a redox protein is one of the most important perceptions for the development of next-generation biosensor devices.[9] Flavin adenine dinucleotide (FAD)/$FADH_2$ present at the prosthetic group of glucose oxidase (GO_x) is known to be the active redox species, but it is deeply enclosed inside the nonconducting layer of rigid protein (GO_x) structure.[9,10]

Metal−organic framework (MOF) shows promising diversity and fascinated scientific community for its exclusive framework design, large surface-to-volume ratio, and tunable pore sizes.[11] Zinc-imidazole framework 8 (ZIF-8) is a subclass of zeolitic MOF. ZIF-8 is a well-known microstructure due to its unique cavity and tunable pore size to accommodate small to large biomolecules and protect them from major external stimuli.[12−20] On the other hand, metal nanoparticles possess exceptional physical and chemical properties and can be used as a component of composite as it possesses high surface area, which assists in reducing the electron tunneling distance.[21−26] Tandem catalysis is one of the interesting properties of a catalyst. If a single catalyst can govern two concurrent reactions, it is called a tandem catalyst. GO_x encapsulated into MOF moiety can act as tandem catalyst for glucose

Received: August 10, 2018
Accepted: October 24, 2018
Published: November 1, 2018

DOI: 10.1021/acsomega.8b01968
ACS Omega 2018, 3, 14634−14640

oxidation and H_2O_2 reduction.[27] TiO_2 nanoparticle is known to have high charge-storage ability due to high double-layer capacitance. Using the same, there are reports where TiO_2 had been used as an active catalyst for nonenzymatic biosensor. The double-layer capacitance of TiO_2 can be used as an effective source for charge-transfer agent at electrode−electrolyte interface.[9,28,29]

In this work, we have proposed an innovative protocol to encapsulate both TiO_2 and GO_x jointly inside the cavity of ZIF-8 to fabricate the as-synthesized nanocomposite GO_x@ZIF-8(TiO_2) and successfully utilize the same for the tandem glucose sensor application. The as-synthesized material is drop-cast on a glassy carbon electrode (GCE), and amperometry was performed to obtain the sensor response. The composite shows a detection limit as low as 80 nM of glucose, which accredits the monitoring of glucose from sweat. Commercially available TiO_2 nanopowder has been used after probe sonication. Moreover, the catalyst shows tandem catalytic behavior to both glucose oxidation and peroxide reduction simultaneously. The oxidation of glucose to gluconate was also confirmed by standard colorimetric experiment by assaying glucose with glucose oxidase−peroxidase (GOD−POD) moiety. The redox adjustment of the couple FAD/$FADH_2$ makes the catalyst different toward sophisticated glucometer fabrication. This is the very first time that both a semiconductor nanoparticle and an enzyme are encapsulated into an MOF cavity. The presented work also envisaged low-level detection of glucose (80 nM), which is significantly low compared to the previously reported TiO_2-based glucose sensor.

2. RESULTS AND DISCUSSION

2.1. Characterization of Materials. The as-synthesized GO_x@ZIF-8(TiO_2) material shows characteristic features due to the presence of crystalline TiO_2. Powder X-ray diffraction (PXRD) was performed to determine the phases of the synthesized probe after the compound was vacuum-dried for 24 h. The PXRD spectra of the as-synthesized GO_x@ZIF-8(TiO_2) are depicted in red in Figure 1. The PXRD spectra of

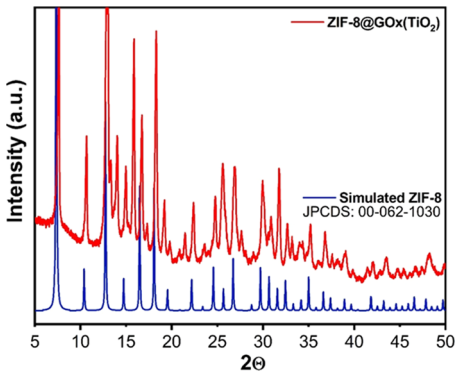

Figure 1. PXRD patterns of synthesized GO_x@ZIF-8(TiO_2) along with simulated ZIF-8 (JCPDS: 00-062-1030) GO_x for comparison.

the as-synthesized composite are compared to the simulated PXRD data of the standard ZIF-8, as depicted in blue of the same figure. It is clearly visible from the PXRD comparison data that there is a >95% PXRD peak matching of the synthesized probe compared to the standard peaks of ZIF-8, suggesting that the native structural property of ZIF-8 remains intact after the encapsulation of TiO_2 and GO_x. Two distinct peaks at 25.36 and 48.17° confirm the presence of anatase TiO_2 (JCPDS: 21-1272).[30] The standard basal plane of TiO_2 (200) at 48.17° estimated from the XRD data is correlated perfectly with the TEM result.

Field emission scanning electron microscopy (FE-SEM) was done to investigate the surface morphology of GO_x@ZIF-8(TiO_2) and is depicted in Figure 2A, which represents a distinct flowerlike structure having many sheets at low magnification. At high magnification, a hexagonal sheet was observed, as depicted in Figure 2B. The morphology reveals high surface area of the probe due to the presence of TiO_2 nanopowder. GO_x is supposed to play a vital role along with TiO_2 in governing the morphology. It was previously known that GO_x has an affinity toward imidazole by hydrophobic interaction and hydrogen bonding.[27] Moreover, imidazole is considered to be the building block of ZIF-8, and hence GO_x controls the morphology of the as-synthesized probe. Further, transmission electron microscopy (TEM) was performed to investigate the spatial structure of the synthesized microstructure and is depicted in Figure 2C. Distinctive lattice fringes were observed, probably depicting the presence of TiO_2. High-resolution transmission electron microscopy (HR-TEM) was performed to obtain the plane of TiO_2 lattice, and the result is depicted in Figure 2D. The HR-TEM image shows the presence of (200) plane of anatase TiO_2 with distinct metal fringes and a *d*-spacing of 0.189 nm.

The result also matches with the PXRD data, which confirms the presence of (200) plane of TiO_2. Scanning transmission electron microscope−energy-dispersive X-ray spectroscopy (STEM−EDX) had been done to get further concrete information regarding the encapsulation of TiO_2 into ZIF-8 moiety, and the result is depicted in Figure S1 (Supporting Information). The result depicts that the TiO_2 nanoparticle is distributed homogeneously with an almost equal spatial distance within the cavity of ZIF-8 microstructure.

ZIF-8 possesses tunable pore size, which can accommodate biomolecules. Fourier transform infrared spectroscopy (FT-IR) had been performed to check whether GO_x possesses its native structure after encapsulation. The FT-IR spectrum is depicted in Figure 3. Characteristic IR peaks for GO_x are observed at 1651 and 1420 cm^{-1}. The peak at 1651 cm^{-1} is considered to be the stretching vibration of peptidic −C═O group of amide-I, whereas the peak at 1420 cm^{-1} corroborates the in-plane bending vibration of N_5H in FAD group.[31] It can be clearly seen from the FT-IR spectrum that 1654 cm^{-1} peak of amide-I slightly shifted to 1651 cm^{-1}. The resultant shift is due to the effect of amide-I, which is already reported to be highly sensitive toward structural modification.[32]

One of the prime concerns to obtain FT-IR spectra is to validate the presence of GO_x in its native state, and the existence of two peaks at 1651 and 1420 cm^{-1} clearly suggests that GO_x is not degraded by any external stimuli and possesses its native biological structure inside the cavity of ZIF-8 MOF, showing biocatalytic activity.

Thermogravimetric analysis (TGA) had been done to estimate the thermal stability of the as-synthesized probe. The TGA profile is depicted in Figure S2 (Supporting Information). It is clearly seen from Figure S2 (Supporting Information) that there is a steep decrease of weight loss percentage due to MOF decomposition. The weight loss at 165 °C corresponds to the evaporation of occluded water and organic components. The latter corresponds to framework

DOI: 10.1021/acsomega.8b01968
ACS Omega 2018, 3, 14634−14640

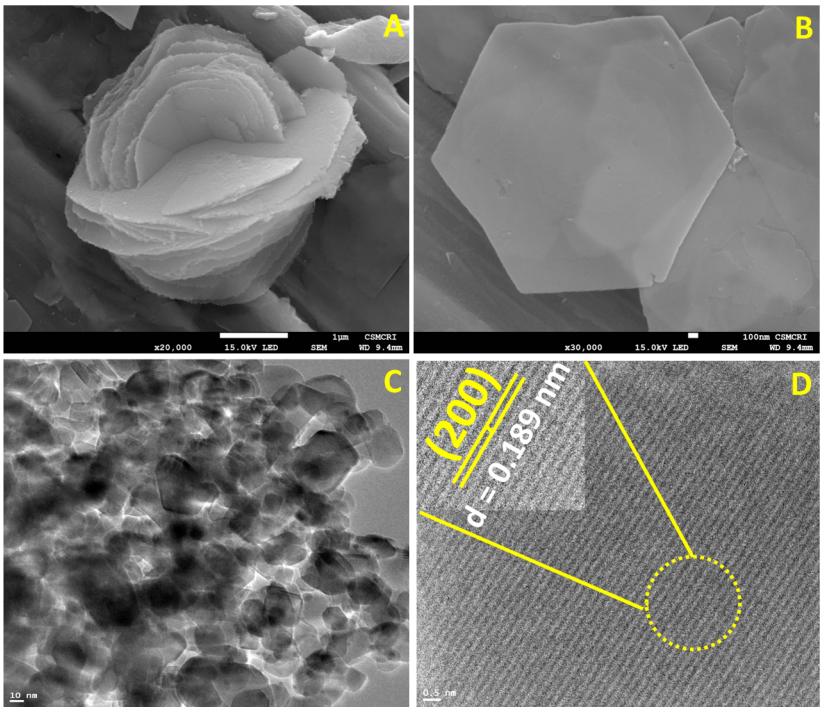

Figure 2. FE-SEM image of synthesized GO_x@ZIF-8(TiO2): (A) Multisheet-assembled growth of the probe; (B) magnified image showing a hexagonal single sheet having large surface area; (C) TEM image of TiO_2 growth-assembled nanoparticles; (D) HR-TEM image of TiO_2 lattice fringes consisting of 200 TiO_2 plane (anatase).

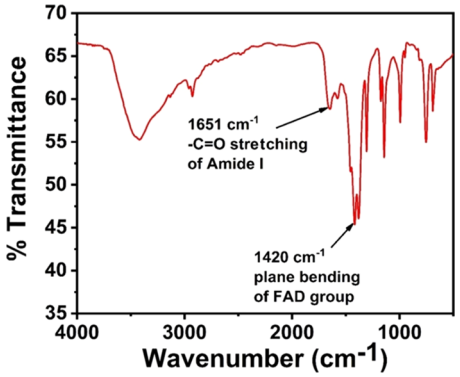

Figure 3. FT-IR spectra of GO_x@ZIF-8(TiO_2) showing distinctive peaks for the presence of glucose oxidase (GO_x) in its native form.

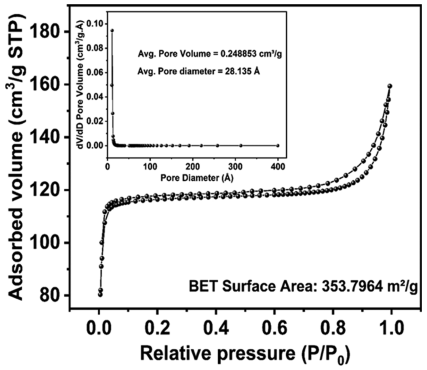

Figure 4. Nitrogen adsorption−desorption isotherm of GO_x@ZIF-8(TiO_2) showing hysteresis at >0.8 P/P_0. The average pore volume and pore diameter are calculated from the BJH plot as depicted in the inset.

degradation. The analysis envisaged the stability profile of the as-synthesized probe, and it can be concluded that the probe is stable up to ∼200 °C.

The nitrogen adsorption−desorption curve was plotted and a hysteresis was observed in the high-pressure region (>0.8 P/P_0), proposing the formation of type IV isotherm, which is associated with capillary condensation taking place in mesopores and the limited uptake over a range of high P/P_0. The initial part of the type IV isotherm is attributed to monolayer−multilayer adsorption since it follows the same path as the corresponding part of the type II isotherm obtained with the given adsorption on the same surface area of the adsorbent in a nonporous form. The adsorption−desorption Brunauer−Emmett−Teller (BET) isotherm is depicted in Figure 4. The BET surface area was measured as 353.8 m^2/g, which is quite superior to that of the previously reported TiO_2 composite. High surface area clearly envisaged uniform encapsulation of GO_x and TiO_2 into the ZIF-8 cavity. To obtain the pore size distribution of the synthesized probe, the Barrett−Joyner−Halenda (BJH) plot was plotted and is depicted in the inset of Figure 4. The average pore volume and pore diameter are found to be 0.248853 cm^3/g (STP) and 28 Å, respectively. The result is attributed to the ability of ZIF-8 matrix to accommodate TiO_2 and GO_x.

2.2. GOD−POD Test to Assay D-Glucose. It has been already shown that GO_x can possess its native structure inside ZIF-8 moiety due to the exceptional tunable pore size of ZIF-8, which accommodates GO_x and protects it from the external chemical stimuli. Furthermore, to check the bioactivity of GO_x inside the ZIF-8 MOF, glucose oxidase−peroxidase (GOD−POD) assay test was done. The general principle of this test is basically the oxidation of glucose to gluconate in the presence of GO_x, which acts as an enzyme. The reaction ends up with the formation of hydrogen peroxide (H_2O_2, eqs 1 and 2),

DOI: 10.1021/acsomega.8b01968
ACS Omega 2018, 3, 14634−14640

which can be uptaken by 4-aminophenazone, a chromogenic oxygen acceptor, and in the presence of phenol, a peroxidase (POD) quinone dye is formed, which shows red color upon completion of the reaction[27]

$$\beta\text{-D-glucose} + O_2 + H_2O \xrightarrow{GO_x} \text{gluconate} + H_2O_2 \quad (1)$$

$$H_2O_2 + \text{phenol} + (\text{4-AP}) \xrightarrow{POD} \text{red quinone dye} + H_2O \quad (2)$$

GOD−POD was performed to examine the activity of the probe with possible interferent analytes like fructose, galactose, lactose, and urea, and the outcome is visible by the naked eye, which is depicted in Figure S3 (Supporting Information). It is clearly visible that the synthesized probe is exclusively selective toward glucose. Characteristic UV−vis absorbance peak at 505 nm wavelength was found, which confirms the presence of GO_x inside the as-synthesized composite probe. The outcome is depicted in Figure S4 (Supporting Information). The result suggests that GO_x is biocatalytically active and definitely encapsulated into ZIF-8 matrix.

2.3. Biosensor Response of GO_x@ZIF-8 (TiO_2). High surface coverage of TiO_2 and the excellent biocatalytic activity of GO_x demonstrate the as-synthesized ZIF-8 composite to be an admirable candidate for the fabrication of glucose biosensor, accrediting a low-level detection of glucose from sweat/saliva. Cyclic voltammetry (CV) technique is used to check the faradic behavior of electrolyte or species attached with electrode, and for this purpose, CV experiment was performed using GO_x@ZIF-8(TiO_2)-modified GCE at a scan rate of 50 mV/s. Prior to use, GCE was polished in a 0.3 μ alumina slurry by putting in a high-mesh pad, followed by ultrasonication in 1:1 ethanol−water mixture for 15 min. Finally, the GCE was washed with Milli-Q water several times and dried under room temperature. The electrode was kept covered to avoid any unavoidable dust particles. The as-synthesized composite (5 mg) was taken and homogeneous dispersion was prepared by taking the same 1 mL of 0.1 M pH 7.4 phosphate-buffered saline (PBS), and the resultant solution was ultrasonicated for 10 min. The resulting dispersion was used as the aliquot for further electrochemical experiment. A small amount of the aliquot (10 μM) was pipetted out using a micropipette and drop-cast over the clean GCE of 5 mm diameter. The electrode was dried at room temperature for 6 h, covered to avoid external dust, and stored overnight at 4 °C.

The tailored electrode was then immersed into a different concentration of glucose in 0.1 M pH 7.4 PBS. The concentration of glucose was increased from 0 to 10 mM, and CV was taken in the range of −0.6 to +0.6 V. Pt wire was used as the counter electrode, and Ag/AgCl (sat. KCl) was used as the reference electrode. A decrement of cathodic current at around −0.45 V vs Ag/AgCl (sat. KCl) was observed while glucose concentration was increased. The result is depicted in Figure 5. The cathodic potential for the possible glucose oxidation is quite similar to that of the other reported catalysts (enzymatic and nonenzymatic). Cathodic peak current was observed to decrease with increasing concentration and plotted against concentration of glucose. A linear increment of anodic current was found with increasing concentration, and the result is depicted in the inset of Figure 5.

The result shows the excellent catalytic activity of the as-synthesized probe to glucose oxidation reaction due to the

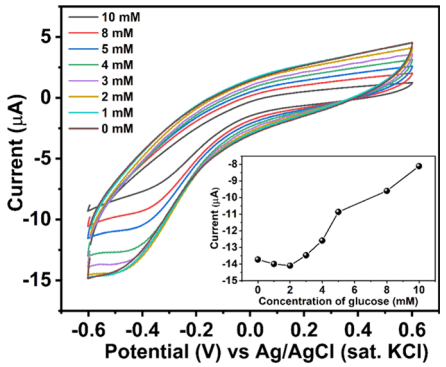

Figure 5. Cyclic voltammetry of synthesized probe with different concentration of glucose in pH 7.4 PBS using a three-electrode cell setup. Calibration of cathodic peak current versus glucose concentration is depicted in the inset.

production of H_2O_2, which results in a decrement of cathodic current/increment of anodic current. Although the nature of the obtained current is nonfaradic (mostly capacitive), the response is well sharp. The possible oxidation reaction occurring at the electrode (GCE)−electrolyte (glucose) interface can be correlated by the following equations (eqs 3 and 4)

$$\text{glucose} + GO_x - FAD \rightarrow \text{gluconate} + GO_x - FADH_2 \quad (3)$$

$$GO_x - FADH_2 + O_2 \rightarrow GO_x - FAD + H_2O_2 \quad (4)$$

The probe GO_x@ZIF-8(TiO_2) not only catalyzes the glucose oxidation reaction but also shows distinctive tandem catalytic property, which makes itself different from other reported amperometric glucose sensors. The probe possesses tandem catalytic activity, which is very unique as it can catalyze the reduction of H_2O_2. A characteristic increase of cathodic current was observed over different concentrations of H_2O_2 at −0.45 V vs Ag/AgCl (sat. KCl). The cathodic current increases due to the possible oxygen reduction reaction occurring at the electrode surface. The result is depicted in Figure S5 (Supporting Information). The possible electrode reaction at the electrode surface is depicted in the following equation (eq 5)

$$GO_x - FAD + H_2O_2 \rightarrow GO_x - FADH_2 + O_2 \quad (5)$$

We have also performed control experiment to understand the role of TiO_2 in this composite, and for this purpose, we synthesized the material without having TiO_2. The synthesized GO_x@ZIF-8 was drop-cast over GCE, and CV was taken in an air-saturated 10 mM glucose solution in pH 7.4 buffer and compared to the CV with GO_x@ZIF-8(TiO_2). The result is depicted in Figure S6. The result clearly suggests that there is an active role of TiO_2 as a charge-storage tank as the control experiment shows an almost nonfaradic linear current−voltage response with mostly the migration of ions present in PBS. The as-synthesized probe is not much affected by ion migration and can store charges originated at the electrode surface due to the generation of H_2O_2, which is uptaken by TiO_2 and transferred to the electrode surface, resulting in the appearance of cathodic peak.

The bioelectrocatalytic activity of the synthesized probe is estimated by calculating electroactive protein density (Γ, mol/cm^2) using eq 6

DOI: 10.1021/acsomega.8b01968
ACS Omega 2018, 3, 14634−14640

$$Q = nFA\Gamma \quad (6)$$

where n, F, and A carry their usual meaning. To calculate Γ, CV was performed in 0.1 M pH 7.4 PBS at a scan rate of 100 mV/s. Γ is calculated to be 1.56×10^{-10} mol/cm^2, which is quite superior to that of other TiO_2-based amperometric glucose sensors.

To estimate the steady-state response of the probe, the potentiostatic amperometric technique was performed. In this technique, the potential needs to be constant while an increment/decrement of current is observed with respect to time. For amperometric glucose measurement, an increment of current is measured with increasing concentration of glucose added at a constant rate. To proceed with the experiment, 0.1 mM glucose has been added successively into the air-saturated pH 7.4 buffer solution. The potential chosen for chronoamperometry was −0.45 V vs Ag/AgCl (sat. KCl), and the result is depicted in Figure 6. Dynamic stairs of current change were

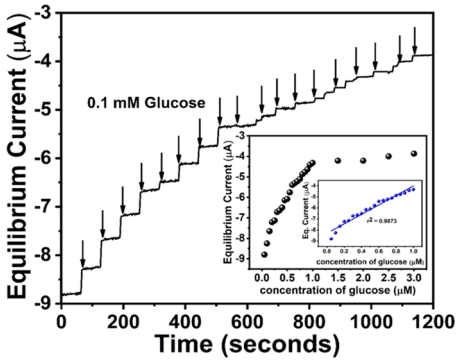

Figure 6. Amperometric response of synthesized probe at −0.45 V vs Ag/AgCl (sat. KCl) by adding 0.1 mM glucose successively in air-saturated pH 7.4 PBS, resulting in a dynamic stair with quick steady state of current. Calibration plot is depicted in the inset.

observed with constant rise and saturation of current. A quick steady state upon successive addition of glucose (∼5 s) was observed, which depicts the efficacy of the probe toward glucose reduction reaction. % Relative standard deviation (RSD) was calculated to check the analytical performance of the synthesized probe, and 1.2% RSD was found for 20 successive dilutions, depicting the nature and stability of the synthesized probe. The steady-state current, obtained from the amperometric plot, was plotted with the change of concentration, and the result is depicted in the inset of Figure 6. A linear calibration plot was obtained, which depicts the linear proportionality of the obtained current with change of concentration. The first rise of current was designated as lower detection limit of this biosensor, and it was calculated at 80 nM glucose concentration. Dissolved oxygen plays an immense role in this experiment as the current achieved steady state gradually after 18 successive dilution. This is probably due to the increment of dissolved oxygen, which vigorously disturbs the FAD/$FADH_2$ equilibrium. This low-level detection of glucose can be strongly correlated with the measurement of blood glucose from sweat/saliva and can be an active component of noninvasive monitor of glucose.

To investigate the tandem catalytic activity of the probe, the same steady-state response for the reduction of H_2O_2 was also investigated, and for this purpose, 0.1 mM H_2O_2 was added successively to the air-saturated pH 7.4 buffer solution. The potential for the chronopotentiometry is also kept fixed, and it was chosen to be the same as we added for glucose monitoring: −0.45 V vs Ag/AgCl (sat. KCl). The current versus time plot was obtained and is depicted in Figure S7 (Supporting Information). The result shows a decrement of cathodic current at −0.45 V vs Ag/AgCl (sat. KCl), which shows the excellent tandem catalytic activity of the probe toward H_2O_2, having a quick steady state of ∼7 s that was achieved successfully.

3. CONCLUSIONS

Herein, we report a protocol for successful encapsulation of TiO_2 and GO_x inside ZIF-8 MOF to synthesize a new probe GO_x@ZIF-8(TiO_2), applicable for mediator-free amperometric detection of glucose. GO_x and TiO_2 are jointly encapsulated into ZIF-8 matrix in aqueous media to form the composite GO_x@ZIF-8(TiO_2). The protocol supports gram-scale synthesis and shows commendable stability and good tandem catalytic activity. The as-synthesized composite was thoroughly characterized by various physicochemical methods. Thermal analysis depicts excellent stability of the probe, whereas X-ray diffraction analysis depicts the crystalline structure of the synthesized probe with TiO_2 nanoparticles in the anatase phase. The presence of TiO_2 nanoparticles increases not only the effective surface area but also the charge storage due to the presence of electrical double layer, which ultimately influences charge transfer at the electrode−electrolyte interface, resulting in excellent tandem catalytic activity toward both glucose oxidation and peroxide reduction reaction. Using this probe, a low-level detection of glucose can be achieved (80 nM) in aqueous media by using very low concentration of GO_x (62 μg in 1 mL), which can be attributed to the monitoring of blood sugar by noninvasive way, mainly from sweat. Overall, the synthetic probe can be demonstrated as competent, robust, and aqueous media-tolerable nanocomposite applicable as tandem catalyst for both glucose oxidation and peroxide reduction reaction.

4. EXPERIMENTAL SECTION

4.1. Materials and Methods. Analytical grades of titanium oxide nanopowder (TiO_2), glucose oxidase from Aspergillus niger (GO_x), and 2-methylimidazole were purchased from Sigma-Aldrich and used without further purification. Analytical-grade $Zn(NO_3)_2{\cdot}6H_2O$ purchased from SRL Chemicals was also used without further purification. The synthesis of GO_x@ZIF-8(TiO_2) nanocomposite was done in aqueous media at room temperature.

The conventional glassy carbon electrode (GCE) of 5 mm diameter had been used as a working electrode for all electrochemical experiments performed. Prior to the experiment, alumina slurry of size 0.3 μ was put in a cloth of dense mesh and the electrode was polished gently, followed by sonication for 15 min in 1:1 ethanol−water mixture to get a clean GCE surface for drop-casting of the as-synthesized composite. The electrode was washed several times with ultrapure Milli-Q water and dried at room temperature prior to use for experiment. A conventional electrolytic cell setup consisting of three electrodes was used in all of the electrochemical experiments. Glassy carbon was utilized as the working electrode, Pt wire (0.1 mm diameter) was used as the counter electrode, and Ag/AgCl (sat. KCl) was used as the reference electrode. The GO_x slurry of GO_x@ZIF-8(TiO_2) composite was prepared for electroanalysis. Material (1 mg) is

DOI: 10.1021/acsomega.8b01968
ACS Omega 2018, 3, 14634−14640

Scheme 1. Schematic Representation for Fabrication of GO_x@ZIF-8(TiO_2)

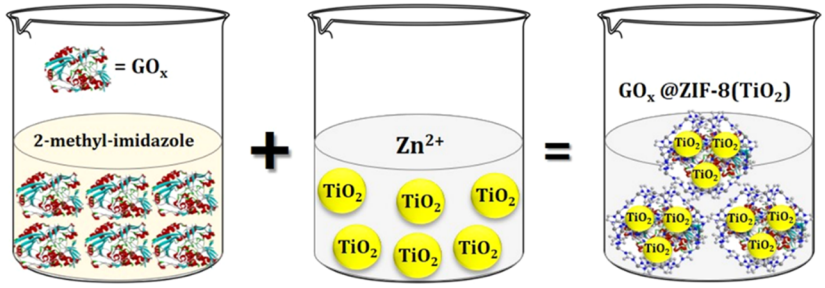

dispersed in 200 μL of pH 7.4 buffer to make the slurry, followed by ultrasonication for 15 min. Furthermore, 5 μL of 0.5% nafion is mixed with the slurry, which acts as a binder to make the material strongly attached to the GCE surface. All of the electrochemical experiments were performed in Metrohm Autolab 203 potentiostat/galvanostat.

The structure of the as-synthesized composite was characterized by various physicochemical techniques. PXRD (PAN Analytical Empyrean Series 2 X-ray diffraction system) was done to investigate the crystal structure of the synthesized probe. The morphology of the synthesized microstructured material was investigated by FE-SEM (JEOL JSM-7100F) and HR-TEM (JEOL JEM-2100). UV−vis spectra were recorded with Varian spectrophotometer. FT-IR experiment was performed using PerkinElmer G-FT-IR. TGA experiment was performed in Mettler Toledo instrument. BET N_2 adsorption−desorption isotherm was measured in Micromeritics, ASAP 2010. The detailed synthetic procedure for the fabrication of GO_x@ZIF-8(TiO_2) nanocomposite is described below. Metrohm Autolab 203 potentiostat/galvanostat is used for all electrochemical measurements.

4.2. Synthesis of GO_x@ZIF-8(TiO_2). ZIF-8 was prepared by a previously reported method.[13] Two distinct synthetic mixtures of 22.70 g of 2-methlyimidazole (108 mM) were dissolved in 400 mL of ultrapure Milli-Q water, and 50 mg of GO_x (8170 units in 50 mg) was added to the same solution, labeled (A). The resulting solution turned pale yellow. In another synthetic mixture, 1.17 g of $Zn(NO_3)_2{\cdot}6H_2O$ (1.53 mM) was dissolved in another 390 mL of ultrapure Milli-Q water separately and labeled (B). TiO_2 nanopowder (5 mg) was taken in 1 mL of Milli-Q water separately (C) and sonicated for 30 min until a homogeneous dispersion formed. The as-prepared (B) and (C) solutions were added directly to the as-prepared mixture (A) under constant stirring of 700 rpm at room temperature, and the total reaction mixture was stirred for 3 h. It was observed that the solution turned hazy from transparent pale yellow, which is the indication for the encapsulation of both GO_x and TiO_2 jointly inside ZIF-8 moiety. The probable haziness may have appeared due to precipitation of the as-synthesized probe. Then, the mixture was allowed to stand overnight in a 100 mL beaker to settle down the desired precipitate. The settled solid precipitate was slowly removed from the beaker using a micropipette and further centrifuged in 10 000 rpm for 10 min. The precipitate was collected and washed thoroughly with 50 mL of Milli-Q water three times to remove excess GO_x and TiO_2, which may have stuck to the surface of the synthesized MOF. Finally, the probe was put in a dessicator and dried under vacuum. An off-white solid composite was recovered, and this is the first initial confirmation for the formation of GO_x@ZIF-8(TiO_2) nanocomposite. The synthetic route is schematically depicted in Scheme 1. The as-synthesized probe was further characterized by various physicochemical techniques like FT-IR, PXRD, FE-SEM, HR-TEM, and UV−vis spectroscopies to confirm the formation of the desired material.

■ ASSOCIATED CONTENT

Supporting Information

The Supporting Information is available free of charge on the ACS Publications website at DOI: 10.1021/acsomega.8b01968.

STEM−EDX mapping of TiO_2 (red color building block) over ZIF-8 layers (green color building block) showing equal spatial distribution of TiO_2 (Figure S1); thermogravimetric analysis of GO_x@ZIF-8(TiO_2) showing distinct degradation region at different temperature (Figure S2) (PDF)

■ AUTHOR INFORMATION

Corresponding Author

*E-mail: dnsrivastava@csmcri.res.in.

ORCID

Divesh N. Srivastava: 0000-0003-1699-4997

Notes

The authors declare no competing financial interest.

■ ACKNOWLEDGMENTS

CSIR-CSMCRI registration No. 108/2018. The funding through project MLP-0018 is gratefully acknowledged. A.P. acknowledges CSIR for Senior Research Fellowship. AESD & CIF Division of CSMCRI is acknowledged for all of the instrumental facilities.

■ REFERENCES

(1) Whiting, D. R.; Guariguata, L.; Weil, C.; Shaw, J. IDF Diabetes Atlas: Global estimates of the prevalence of diabetes for 2011 and 2030. *Diabetes Res. Clin. Pract.* **2011**, *94*, 311−321.

(2) Moncada, S.; Higgs, A. The L-arginine-nitric oxide pathway. *N. Engl. J. Med.* **1993**, *329*, 2002−2012.

(3) Gao, W.; Emaminejad, S.; Nyein, H. Y. Y.; Challa, S.; Chen, K.; Peck, A.; Fahad, H. M.; Ota, H.; Shiraki, H.; Kiriya, D.; Lien, D. H.; Brooks, G. A.; Davis, R. W.; Javey, A. Fully integrated wearable sensor arrays for multiplexed in situ perspiration analysis. *Nature* **2016**, *529*, 509−514.

(4) Lee, H.; Choi, T. K.; Lee, Y. B.; Cho, H. R.; Ghaffari, R.; Wang, L.; Choi, H. J.; Chung, T. D.; Lu, N.; Hyeon, T.; Choi, S. H.; Kim, D. H. A graphene-based electrochemical device with thermoresponsive microneedles for diabetes monitoring and therapy. *Nat. Nanotechnol.* **2016**, *11*, 566−572.

DOI: 10.1021/acsomega.8b01968
ACS Omega 2018, 3, 14634−14640

(5) Bandodkar, A. J.; Jia, W.; Yardimci, C.; Wang, X.; Ramirez, J.; Wang, J. Tattoo-based noninvasive glucose monitoring: a proof-of-concept study. *Anal. Chem.* **2015**, *87*, 394−398.
(6) Rahman, M. M.; Ahammad, A. J. S.; Jin, J.-H.; Ahn, S. J.; Lee, J.-J. A comprehensive review of glucose biosensors based on nanostructured metal-oxides. *Sensors* **2010**, *10*, 4855−4886.
(7) Wang, J. Glucose Biosensors: 40 Years of Advances and Challenges. *Electroanalysis* **2001**, *13*, 983−988.
(8) Wang, J. Electrochemical glucose biosensors. *Chem. Rev.* **2008**, *108*, 814−825.
(9) Bao, S.-J.; Li, C. M.; Zang, J.-F.; Cui, X.-Q.; Qiao, Y.; Guo, J. New nanostructured TiO_2 for direct electrochemistry and glucose sensor applications. *Adv. Funct. Mater.* **2008**, *18*, 591−599.
(10) Liu, J.; He, Z.; Khoo, S. Y.; Tan, T. T. Y. A new strategy for achieving vertically-erected and hierarchical TiO2 nanosheets array/carbon cloth as a binder-free electrode for protein impregnation, direct electrochemistry and mediator-free glucose sensing. *Biosens. Bioelectron.* **2016**, *77*, 942−949.
(11) Furukawa, H.; Cordova, K. E.; O'Keeffe, M.; Yaghi, O. M. The Chemistry and Applications of Metal−Organic Frameworks. *Science* **2013**, *341*, No. 1230444.
(12) Zhong, H. X.; Wang, J.; Zhang, Y. W.; Xu, W. L.; Xing, W.; Xu, D.; Zhang, Y. F.; Zhang, X. B. ZIF-8 derived graphene-based nitrogen-doped porous carbon sheets as highly efficient and durable oxygen reduction electrocatalysts. *Angew. Chem., Int. Ed.* **2014**, *53*, 14235−14239.
(13) Pan, Y.; Liu, Y.; Zeng, G.; Zhao, L.; Lai, Z. Rapid synthesis of zeolitic imidazolate framework-8 (ZIF-8) nanocrystals in an aqueous system. *Chem. Commun.* **2011**, *47*, 2071−2073.
(14) Lu, G.; Hupp, J. T. Metal−organic frameworks as sensors: a ZIF-8 based Fabry−Pérot device as a selective sensor for chemical vapors and gases. *J. Am. Chem. Soc.* **2010**, *132*, 7832−7833.
(15) Banerjee, R.; Furukawa, H.; Britt, D.; Knobler, C.; O'Keeffe, M.; Yaghi, O. M. Control of Pore Size and Functionality in Isoreticular Zeolitic Imidazolate Frameworks and their Carbon Dioxide Selective Capture Properties. *J. Am. Chem. Soc.* **2009**, *131*, 3875−3877.
(16) Liu, H.; Liu, Y.; Li, Y.; Tang, Z.; Jiang, H. Metal−Organic Framework Supported Gold Nanoparticles as a Highly Active Heterogeneous Catalyst for Aerobic Oxidation of Alcohols. *J. Phys. Chem. C* **2010**, *114*, 13362−13369.
(17) Wang, B.; Côté, A. P.; Furukawa, H.; O'Keeffe, M.; Yaghi, O. M. Colossal cages in zeolitic imidazolate frameworks as selective carbon dioxide reservoirs. *Nature* **2008**, *453*, 207−211.
(18) Lu, G.; Li, S.; Guo, Z.; Farha, O. K.; Hauser, B. G.; Qi, X.; Wang, Y.; Wang, X.; Han, S.; Liu, X.; Duchene, J. S.; Zhang, H.; Zhang, Q.; Chen, X.; Ma, J.; Loo, S. C. J.; Wei, W. D.; Yang, Y.; Hupp, J. T.; Huo, F. Imparting functionality to a metal−organic framework material by controlled nanoparticle encapsulation. *Nat. Chem.* **2012**, *4*, 310−316.
(19) Banerjee, R.; Phan, A.; Wang, B.; Knobler, C.; Furukawa, H.; O'Keeffe, M.; Yaghi, O. M. High-throughput synthesis of zeolitic imidazolate frameworks and application to CO_2 capture. *Science* **2008**, *319*, 939−943.
(20) Hu, Y.; Liao, J.; Wang, D.; Li, G. Fabrication of Gold Nanoparticle-Embedded Metal−Organic Framework for Highly Sensitive Surface-Enhanced Raman Scattering Detection. *Anal. Chem.* **2014**, *86*, 3955−3963.
(21) Liu, S.; Ju, H. Reagentless glucose biosensor based on direct electron transfer of glucose oxidase immobilized on colloidal gold modified carbon paste electrode. *Biosens. Bioelectron.* **2003**, *19*, 177−183.
(22) Zhai, D.; Liu, B.; Shi, Y.; Pan, L.; Wang, Y.; Li, W.; Zhang, R.; Yu, G. Highly sensitive glucose sensor based on Pt nanoparticle/polyaniline hydrogel heterostructures. *ACS Nano* **2013**, *7*, 3540−3546.
(23) Sakslund, H.; Wang, J.; Lu, F.; Hammerich, O. Development and evaluation of glucose microsensors based on electrochemical codeposition of ruthenium and glucose oxidase onto carbon fiber microelectrodes. *J. Electroanal. Chem.* **1995**, *397*, 149−155.
(24) Mazeiko, V.; Kausaite-Minkstimiene, A.; Ramanaviciene, A.; Balevicius, Z.; Ramanavicius, A. Gold nanoparticle and conducting polymer-polyaniline-based nanocomposites for glucose biosensor design. *Sens. Actuators, B* **2013**, *189*, 187−193.
(25) Gao, Z. D.; Guo, J.; Shrestha, N. K.; Hahn, R.; Song, Y. Y.; Schmuki, P. Nickel Hydroxide Nanoparticle Activated Semi-metallic TiO2 Nanotube Arrays for Non-enzymatic Glucose Sensing. *Chem. - Eur. J.* **2013**, *19*, 15530−15534.
(26) Luo, W.; Zhu, C.; Su, S.; Li, D.; He, Y.; Huang, Q.; Fan, C. Self-catalyzed, self-limiting growth of glucose oxidase-mimicking gold nanoparticles. *ACS Nano* **2010**, *4*, 7451−7458.
(27) Wang, Q.; Zhang, X.; Huang, L.; Zhang, Z.; Dong, S. GOx@ZIF-8(NiPd) Nanoflower: An Artificial Enzyme System for Tandem Catalysis. *Angew. Chem., Int. Ed.* **2017**, *130022*, 16082−16085.
(28) Chandra, R.; Mukhopadhyay, S.; Nath, M. TiO_2@ZIF-8: A novel approach of modifying micro-environment for enhanced photocatalytic dye degradation and high usability of TiO_2 nanoparticles. *Mater. Lett.* **2016**, *164*, 571−574.
(29) Pipelzadeh, E.; Rudolph, V.; Hanson, G.; Noble, C.; Wang, L. Photoreduction of CO2 on ZIF-8/TiO2 nanocomposites in a gaseous photoreactor under pressure swing. *Appl. Catal., B* **2017**, *218*, 672−678.
(30) Theivasanthi, T.; Alagar, M. Titanium Dioxide (TiO_2) Nanoparticles XRD Analyses: An Insight. 2013, arXiv preprint arXiv:1307.1091. arXiv.org e-Print archive. https://arxiv.org/abs/1307.1091.
(31) Gutierrez, F.; Rubianes, M. D.; Rivas, G. A. Dispersion of multi-wall carbon nanotubes in glucose oxidase: Characterization and analytical applications for glucose biosensing. *Sens. Actuators, B* **2012**, *161*, 191−197.
(32) Hereć, M.; Gagoś, M.; Kulma, M.; Kwiatkowska, K.; Sobota, A.; Gruszecki, W. I. Secondary structure and orientation of the pore-forming toxin lysenin in a sphingomyelin-containing membrane. *Biochim. Biophys. Acta, Biomembr.* **2008**, *1778*, 872−879.

DOI: 10.1021/acsomega.8b01968
ACS Omega 2018, 3, 14634−14640